Lateral stirring in the ocean on scales of 0.1-10 km: The role of internal waves

M.-Pascale Lelong, Jeffrey J. Early, Eric Kunze, Miles A. Sundermeyer and Cimarron J. Wortham

NorthWest Research Associates,
Redmond, Washington USA
pascale@nwra.com

Abstract

High values of lateral diffusivity, O(1) m^2 s^{-1}, on horizontal scales of 0.1-10 km are routinely found in the stratified ocean interior, irrespective of ambient mesoscale strain rate, yet the primary dynamical mechanism responsible for this behavior has not been established. Theoretical arguments combined with numerical simulations using both a nonlinear Boussinesq model and a linear internal wave model suggest that Stokes drift driven by a weakly nonlinear Garrett-Munk internal wave field can significantly enhance lateral diffusivity. In this note, we illustrate the dispersive role of internal-wave-driven Stokes drift for several stratification profiles and positions in the water column and also consider scale-dependent dispersion in submesoscale fields that include both vortices and internal waves.

1 Introduction

Dye-tracer-release experiments in the stratified ocean interior find values of isopycnal diffusivities of O(1) m^2s^{-1} on scales of 0.1-10 km (Ledwell et al., 1993; Sundermeyer and Ledwell, 2001). Tracer releases at two separate sites in the Sargasso Sea during the June 2011 ONR Lateral Mixing experiment (LatMix11, Shcherbina et al. (2015)) also inferred submesoscale isopycnal diffusivities in this range even though background mesoscale strain rates at the two sites differed by an order of magnitude. The consistent range of submesoscale isopycnal diffusivities recorded under different mesoscale conditions leads us to hypothesize that internal waves, ubiquitous in the ocean, are responsible for the observed submesoscale isopycnal dispersion in LatMix11. The focus of the study presented here is on explaining observations in regions where the geostrophic strain-rate is weak. Our numerical approach consists of isolating different potential dynamical mechanisms by means of linear and nonlinear simulations of particle and dye dispersion in fields consisting of waves and vortices. In the next section, we briefly review and contrast three internal-wave-driven mechanisms that might contribute to lateral dispersion at the submesoscale. The numerical method is presented in Section 3, followed by results in Section 4 and conclusions in Section 5.

Three possible internal-wave-driven mechanisms that can influence isopycnal diffusivities are: (i) internal-wave shear dispersion (Young et al., 1982; Kunze and Sundermeyer, 2015), (ii) vortical-mode stirring (Sundermeyer, 1998; Sundermeyer and Ledwell, 2001; Sundermeyer and Lelong, 2005) and (iii) internal-wave-induced dispersion (Holmes-Cerfon et al. (2011); Bühler et al. (2013); Early et al. (*in prep*)). Effective horizontal diffusivity κ_h for mechanisms (i) and (ii) is proportional to $(N/f)^2\kappa_z$, in contrast to the scaling for mechanism (iii) which is independent of κ_z and varies as N^2/f. Here, N and f denote buoyancy and inertial frequencies and κ_z the diapycnal diffusivity. Whereas (i) and (iii) can be active in linear and nonlinear regimes, (ii) represents an inherently nonlinear process. The

linear/nonlinear character will also be exploited to identify the source of lateral dispersion. The difference in scaling can help identify the dynamics most likely to be acting in LatMix11 at Site I where the flow was dominated by weakly nonlinear internal waves. Verifying the scaling of effective diffusivity requires a sweep of parameter space beyond the scope of this short note. Here, we will limit ourselves to illustrating the differences in dye/particle dispersion as a function of initial position relative to flow boundaries in linear and nonlinear flows combining internal-wave and geostrophic components.

Internal-wave shear dispersion refers to the enhanced isopycnal diffusion resulting from the interaction of molecular diapycnal diffusion and internal-wave vertical shear (Young et al., 1982). When the vertical shear is due to a broadband internal-wave field, this interaction results in an effective lateral diffusivity κ_h which scales as $(N/f)^2\kappa_z$ where κ_z is the turbulent diapycnal diffusivity. An important caveat is that past estimates of internal-wave-driven shear dispersion have not taken into account the highly intermittent nature of turbulent mixing and internal-wave shear magnitude, correlated due to episodic internal-wave-breaking. When this intermittency is taken into consideration, substantially higher dispersion is predicted that is more in line with observed inferences (Kunze and Sundermeyer, 2015).

Vortical-mode production away from topography is primarily due to breaking internal waves, a highly nonlinear process. Breaking internal waves produce patches of PV anomaly which give rise to patch-scale vortices (vortical modes). Sundermeyer (1998) predicted that the effective lateral diffusivity due to stirring by vortical modes would also scale as $(N/f)^2\kappa_z$. (Polzin, 2004; Sundermeyer and Lelong, 2005). This scaling prediction was, by and large, validated with numerical simulations (Sundermeyer and Lelong, 2005).

Alternatively, wave-induced dispersion, also known as Stokes drift, is an inherent wave property and refers to the net mean drift that arises at second-order in wave amplitude. Stokes drift is the difference in a particle's velocity computed in Eulerian and Lagrangian reference frames. While a single infinite plane internal wave has no associated Stokes drift, this is not true in the presence of boundaries (e.g. the sea surface) which set up standing modes, or when the flow consists of combinations of plane waves (e.g a normal mode or a wave packet). Dewar (1980) recognized that Lagrangian floats in a field of Garrett-Munk internal waves would experience non-negligible drift and calculated an internal-wave-induced absolute diffusivity of O(100) $\mathrm{m}^2\ \mathrm{s}^{-1}$. Thorpe (1968) and Gil and Fringer (2011, in revision) computed Lagrangian particle trajectories and the horizontal mass transport due to a mode-1 internal gravity wave in the nonrotating fluid and also concluded that linear internal waves are capable of efficient dispersion.

2 Methods

Our strategy for identifying the source of dispersion in our numerical simulations consists of eliminating one or more contending internal-wave processes described in the previous section. We use a combination of theoretical predictions, and numerical simulations with a three-dimensional spectral nonlinear Boussinesq model **flow_solve** (Winters and de la Fuente, 2012) and a purely linear inviscid internal wave model (Early et al. (2016), *in preparation*). Nonlinear and linear simulations with **flow_solve** are contrasted to isolate linear mechanisms (Stokes drift or shear dispersion). Non-diffusive Lagrangian particles and a diffusive passive tracer are employed concurrently to isolate mechanisms that rely on

diapycnal diffusivity κ_z, namely internal-wave shear dispersion and vortical-mode stirring, from Stokes drift which does not. This note is intended to illustrate some of the mechanisms we have identified, but is by no means exhaustive. More elaborate experiments and detailed analysis are ongoing.

3 Results

In this section, we first contrast IW Stokes drift velocities in flow fields associated with a few normal modes under three different conditions: (1) constant, (2) exponential and (3) realistic summer Sargasso Sea stratification. Next, we compare the effective lateral diffusivities calculated from the second moment of dye variance and mean-square displacements of Lagrangian particles in both linear and nonlinear simulations under identical flow conditions consisting of a broadband GM internal wave field and PV modes, and examine dispersion characteristics at two different depths.

3.1 Impact of stratification

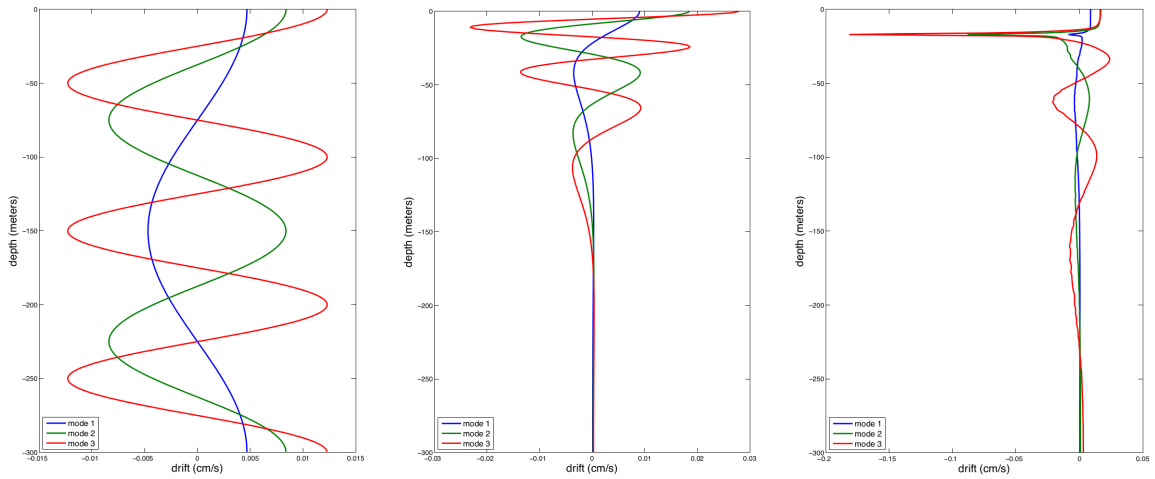

Figure 1: Theoretical Stokes drift velocities induced by a rightward-propagating mode-1 (blue), mode-2 (green), mode-3 (red) internal waves in constant stratification (left), exponential stratification (middle) and summertime Sargasso Sea stratification (right).

To illustrate the impact of stratification and initial vertical position, we compare theoretical Stokes drifts for the first three modes (Figure 1). For the purpose of this exercise, the three modes are chosen to have equal energy. Immediately evident is that Stokes drift is a strong function of both stratification and position in the water column. For constant stratification, the drift velocity is either with or against the direction of phase propagation, depending on the initial particle depth. The net result is zero depth-integrated mass transport. In this example, maximum drift velocity $\approx \pm 0.0125$ cm/s due to mode-3. For exponential stratification, maximum drift velocity is again due to mode 3 and roughly twice as large as for constant stratification, occurring in opposite directions at the surface and slightly below. Drift is negligible below 150 m depth. The presence of a sharp pycnocline in the summer Sargasso Sea case enhances the mode-3 Stokes drift by an order of magnitude within the region of maximum stratification. Large Stokes drifts were also found by Gil and Fringer (in revision) in the presence of sharp density gradients. All dye injections during LatMix11 were made immediately below the base of the mixed layer in a

shallow pycnocline with buoyancy frequency N $\approx 2\times10^{-2}$ rad s^{-1}. This choice of injection depth may explain the effective lateral diffusivities recorded during that experiment.

Effective lateral diffusivity in a submesoscale flow field: We now examine stirring in a realistic simulated ocean flow, using both dye-tracer and Lagrangian particles to identify mechanisms responsible for lateral dispersion. Linear and nonlinear simulations are performed with identical initial conditions in a numerical domain of dimensions 15 km $\times$ 15 km $\times$ 300 m. Stratification is exponential. The Nyquist vertical scale is $\approx$ 5 m, too large to resolve O(1 m) wave breaking scales. Our initial condition is a quasi-stationary flow field containing both internal waves and geostrophic motions. At t = 0, a strip of dye, uniform in y and Gaussian in x and z, is placed at 60 m depth. Concurrently, 100 Lagrangian particles are deployed on a regular grid in a square spanning (6.5 km $<$ x $<$ 8.75 km, 6.5 km $<$ y $<$ 8.75 km) at the same depth as the dye. The initial particle positions span the width but not the length of the dye streak. All simulations are unforced and run for at least 6 days.

Horizontal and vertical effective diffusivities can be inferred from the temporal variation of the second moment of dye concentration σ_x^2 and σ_z^2 (e.g. Sundermeyer and Lelong (2005)). The horizontal effective diffusivity is

$$\kappa_H = \frac{1}{2}\frac{\partial \sigma_x^2}{\partial t}, \tag{1}$$

with a similar expression governing the effective vertical diffusivity κ_z. An effective lateral diffusivity can also be computed from the relative separation of N particles in time. To compare with dye diffusivity, we only consider relative particle separation in the x-direction,

$$\kappa_H = \frac{1}{2}\frac{\partial R}{\partial t} \tag{2}$$

where $R(t) = \frac{1}{N-1}\sum_{i=1}^{N}(x_i - x_{com})^2$ is the mean-square separation in x of particles relative to their center-of-mass (x_{com}, y_{com}).

The evolution of the dye at 60 m depth is shown in Figure 2. At early times, dye diffusion is primarily in the x-direction and governed by the low background (imposed) diffusivity. By day 2, there is evidence of dynamical stirring breaking up homogeneity in the y-direction on scales of $\approx$ 1 km. By day 4, larger meanders with scales of $\approx$ 5 km are visible and distort the dye, eventually breaking it up by day 6.

The dispersion characteristics of dye and particles are shown in Figure 3. Both dye and particle second moments grow exponentially at early times. The dye second moments begin to grow in response to the numerical diffusivity at the grid scale. Linear and nonlinear cases are indistinguishable in this regime. Early on, the dispersion for the particles in the linear simulation appears anomalously low compared to its nonlinear counterpart and to that of the dye in both linear and nonlinear simulations. However, a comparison of the slopes between the two dash-dotted lines indicates that, for the same range of scales, the slopes are within a factor of 2. Suppression of nonlinearities explains the relatively long initial slow-growth phase of particle dispersion in the linear simulation.

Vertical diffusivities inferred from linear dye and particle simulations show a clear increase from background vertical diffusivity whereas the nonlinear cases do not. Linear dye and particles yield comparable vertical diffusivities (as evidenced by the slopes of

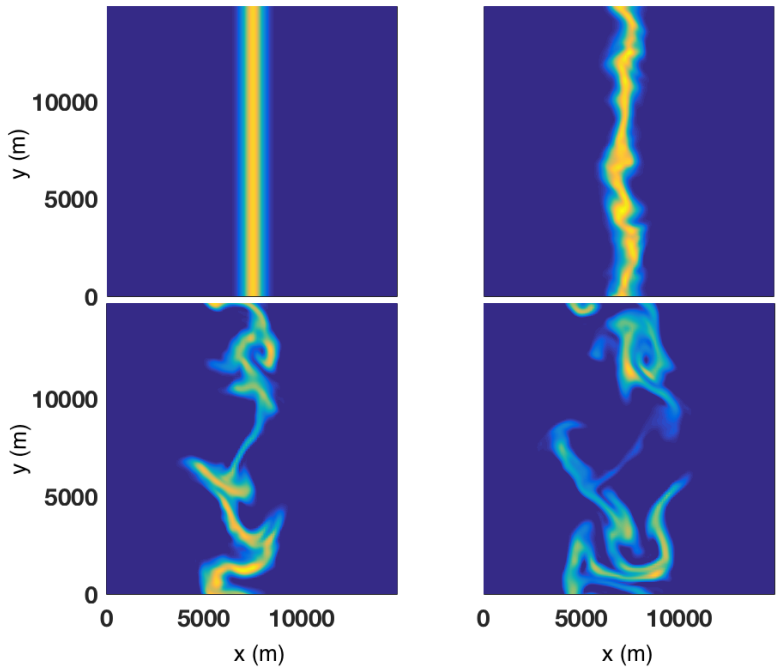

Figure 2: Evolution of a strip of dye placed at 60 m in the nonlinear simulation, at t = 0 (top left), 2 days (top right), 4 days (bottom left), 6 days (bottom right). The colormap is fixed and ranges from 0 (dark blue) to 1 (orange).

dye second moment and particle separation). The different dispersion behavior in the linear and nonlinear simulations is explained by the fact that the linear equations do not constrain dye and particles to isopycnal surfaces and this behavior manifests itself as a nonzero vertical diffusivity. In the nonlinear case, both dye and particles must remain on isopycnals and vertical diffusivity is negligible.

Scale-dependent diffusivity: A plot of diffusivity as a function of relative particle separation (Figure 4) illustrates its scale dependence. At 2 km separation, linear and nonlinear runs exhibit diffusivities of 2.5 and 5 m^2s^{-1} respectively. Second moments of the dye concentration in this regime grow at the same rate in linear and nonlinear simulations, and a dye diffusivity of 4.2 m^2s^{-1} is inferred from the common slope of their second moments (magenta line in Figure 3). Below the 2 km scale, the dispersion is governed by weakly nonlinear processes. In weakly nonlinear flows, the dominant scales of wave and geostrophic components can be identified with variance-preserving spectra of horizontal divergence (waves) and linear PV (vortical modes). In order to compare quantities with the same units, we plot horizontal divergence and absolute vorticity (Figure 6). This is justified since linear PV and absolute vorticity spectra exhibit the same peaks. Vortical motions are present at all scales, with the bulk of their variance at scales larger than 2 km. Waves are concentrated more narrowly around scales of $\approx$ 1.5 km. Below the 1 km scale, waves constitute the only motions while vortical motions are comparable to waves at scales larger than 5 km. Frequency spectra (not shown) confirm that absolute vorticity is concentrated at low frequencies and horizontal divergence at frequencies greater than f.

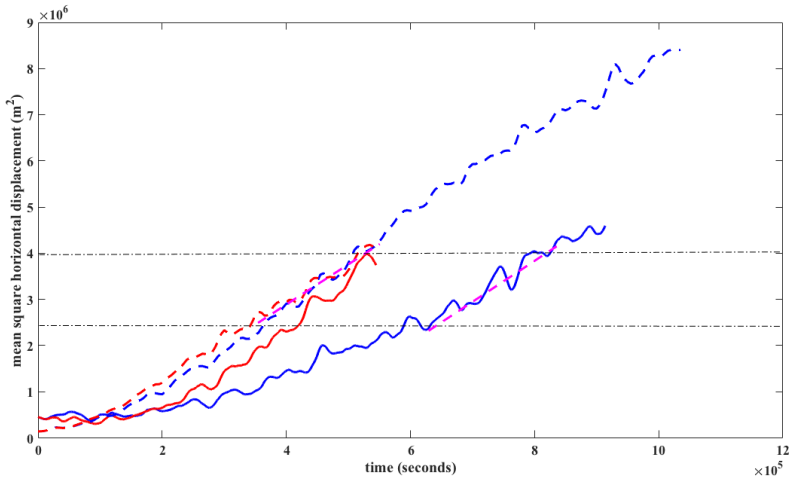

Figure 3: Horizontal dispersion characteristics for dye/particles initially at 60 m depth in linear/nonlinear simulations: dye (linear, dashed blue; nonlinear, dashed red) and particles (linear, solid blue; nonlinear, solid red). Horizontal dash-dotted grey lines delimit the range of spatial scales between1.5 km to 2 km. The two magenta dashed lines have equal slopes.

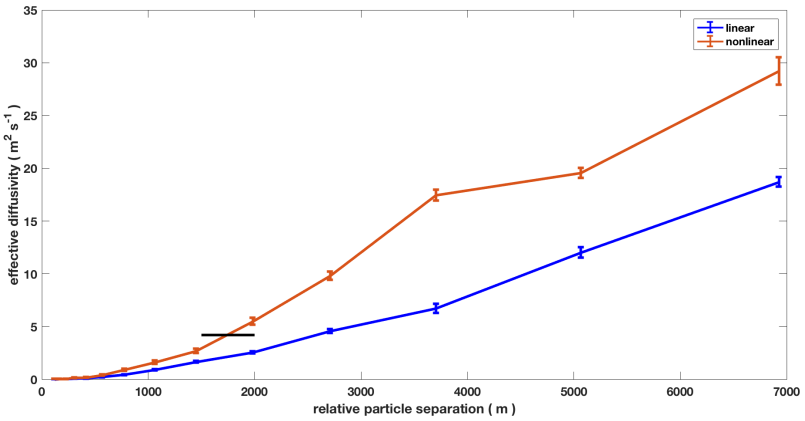

Figure 4: Diffusivity as a function of relative particle separation for linear (blue) and nonlinear (red) simulations. The black line indicates the dye diffusivity at that scale range, inferred from Figure 3 .

4 Conclusion

We have demonstrated that Stokes drift due to single wave modes can result in large horizontal displacements, depending on where particles are placed in the water column (Figure 1). In internal-wave-dominated flows characteristic of quiescent regions such as the Sargasso Sea in early summer, dye and particle horizontal diffusivities agree to within a factor of two in linear and nonlinear simulations (Figure 3). This indicates that the dominant stirring mechanism is linear. In the vertical, dye and particles disperse at the same rate, but linear and nonlinear simulations yield different diffusivities (Figure 5). The fact that horizontal diffusivity is not affected by changes in vertical diffusivity suggests that shear dispersion is not important. Therefore, Stokes drift by linear waves cannot be ruled out but neither can stirring by vortical modes which are present, though not dominant (Figure 6), at all spatial scales.

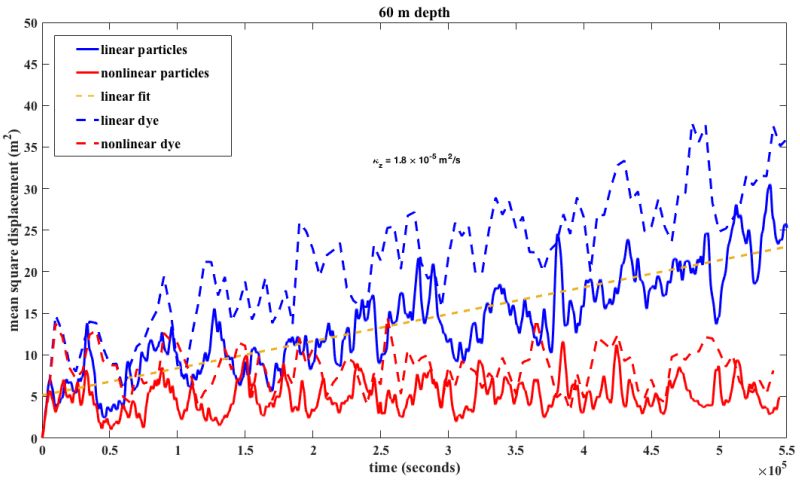

Figure 5: Vertical diffusivities for linear (blue)/nonlinear (red) dye and particles initially placed at 60 m depth.

Acknowledgments: We thank Kraig Winters for the generous use of his numerical code. Support for this work was provided by Office of Naval Research grant N00014-15-1-2465, and National Science Foundation award OCE-1536747.

References

Bühler, O., Grisouard, N., and Holmes-Cerfon, M. (2013). Strong particle dispersion by weakly dissipative random internal waves. *J. Fluid Mech.*, 719:R4 (1–11).

Dewar, W. (1980). The effect of internal waves on neutrally buoyant floats and other near lagrangian tracers. Master's thesis, MIT.

Gil, G. T. and Fringer, O. B. (2011). Lagrangian and Eulerian-mean effects in progressive internal gravity waves. *submitted*.

Holmes-Cerfon, M., Bühler, O., and Ferrari, R. (2011). Particle dispersion by random waves in the rotating boussinesq system. *J. Fluid Mech.*, 670:150–175.

Kunze, E. and Sundermeyer, M. A. (2015). The role of intermittency in internal-wave shear dispersion. *J. Phys. Oceanogr.*, 45:2979–2990.

Ledwell, J., Watson, A., and Law, C. (1993). Evidence for mixing across the pycnocline from an open ocean tracer release experiment. *Nature*, 364(6439):701–703.

Polzin, K. (2004). A heuristic description of internal-wave dynamics. *J. Phys. Oceanogr.*, 34:214–230.

Shcherbina, A. Y., Sundermeyer, M. A., Kunze, E., Eric D'Asaro, a. G. B., Birch, D., Brunner-Suzuki, A.-M. E. G., Callies, J., Cervantes, B. T. K., Claret, M., Concannon, B., Early, J. J., Ferrari, R., Goodman, L., Harcourt, R. R., Klymak, J. M., Lee, C. M., Lelong, M.-P., Levine, M. D., Lien, R.-C., Mahadevan, A., McWilliams, J. C., Molemaker, M. J., Mukherjee, S., Nash, J. D., Özgökmen, T., Pierce, S. D., Ramachandran, S., Samelson, R. M., Sanford, T. B., Shearman, R. K., Skyllingstad, E. D., Smith, K. S., Taylor, A. T. J. R., Terray, E. A., Thomas, L. N., and Ledwell, J. R. (2015). The

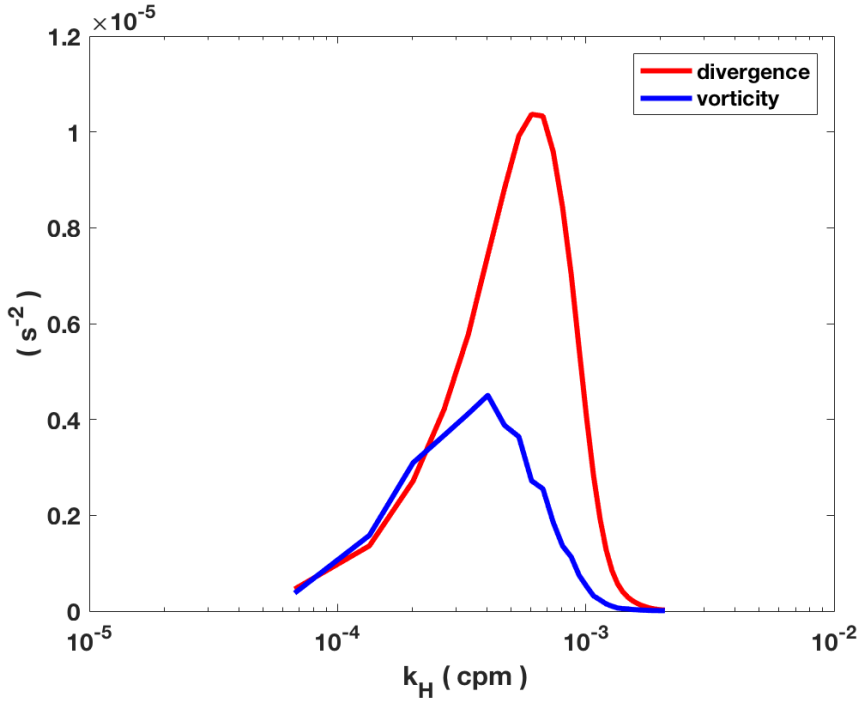

Figure 6: Time-averaged, variance-preserving horizontal-wavenumber spectra of horizontal divergence (red) and absolute vertical vorticity: relative + planetary (blue) for the nonlinear run. The variance in each component is proportional to the area under each curve. Peaks indicate the scales that contribute most of the variance.

LatMix Summer Campaign: Submesoscale Stirring in the Upper Ocean. *Bull. Amer. Meteor. Soc.*, 96:1257–1279.

Sundermeyer, M. A. (1998). *Studies of lateral dispersion in the ocean.* PhD thesis, Massachusetts Institute of Technology / Woods Hole Oceanographic Institution Joint Program.

Sundermeyer, M. A. and Ledwell, J. R. (2001). Lateral dispersion over the continental shelf: Analysis of dye-release experiments. *J. Geophys. Res.*, 106(C5):96039622, doi:10.1029/2000JC900138.

Sundermeyer, M. A. and Lelong, M.-P. (2005). Numerical simulations of lateral dispersion by the relaxation of diapycnal mixing events. *J. Phys. Oceanogr.*, 35(12):2368–2386.

Thorpe, S. A. (1968). On the shape of progressive internal waves. *P. Roy. Soc. Lond. A Mat.*, 263:563–614.

Winters, K. B. and de la Fuente, A. (2012). Modelling rotating stratified flows at laboratory-scale using spectrally-based DNS. *Ocean Modell.*, 49-50:47–59.

Young, W. R., Rhines, P. B., and Garrett, C. J. R. (1982). Shear-flow dispersion, internal waves and horizontal mixing in the ocean. *J. Phys. Oceanogr.*, 12:515–527.